Role of Sequence Bias in the Topology of the Multidrug Transporter EmrE

Hassane S. Mchaourab,* Sanjay Mishra, Hanane A. Koteiche, and Sepan H. Amadi

Department of Molecular Physiology and Biophysics, Vanderbilt University, Nashville, Tennessee 37232

Received April 9, 2008; Revised Manuscript Received May 19, 2008

ABSTRACT: EmrE is the prototype of small multidrug resistance transporters and has emerged as a model of membrane protein evolution. Analysis of the distances separating symmetry-related site-specific spin labels, correlation of topological sequence bias to C-terminal orientation, to membrane insertion efficiency, and to resistance to ethidium bromide collectively demonstrate that EmrE monomers adopt a parallel topology in the functional dimer. We propose a coupled insertion and assembly model for EmrE in which the favorable energetics of the parallel dimer interface override topological constraints arising from weak asymmetry in positive charge distribution.

Small multidrug resistance (SMR) transporters in prokaryotes couple translocation of toxic molecules out of the cell to the inward movement of protons down their electrochemical gradient (*1*). Much of the current structural and mechanistic understanding of SMR transporters has emerged from analysis of *Escherichia coli* EmrE (*2*). Each monomer consisting of four transmembrane helices, the EmrE functional unit, is presumed to be a homodimer (*3*). Despite its small size and relative sequence simplicity, a consensus structure of EmrE has been elusive (*4, 5*). Insights from multiple techniques suggest an asymmetric dimer (*6, 7*), although the origin of the asymmetry remains controversial. A dual topology model proposing antiparallel packing of monomers in the dimer, first observed in now retracted crystal structures (*8*), was recently supported by analysis of EmrE orientation in the membrane using C-terminal green fluorescence protein (GFP) and alkaline phosphatase (PhoA) tags (*9*).

While a dual topology model for EmrE has many attractive aspects, a body of existing biochemical data is more consistent with parallel assembly of the monomers (*2, 10–12*). Furthermore, corollaries for folding and membrane insertion pose intriguing questions. Dual topology requires opposite protomers to insert at a 1:1 ratio. If the only determinant of EmrE topology is the tendency of K- and R-rich loops to orient toward the cytoplasm, the positive inside rule (*13*), the realization of equal amounts of oppositely oriented EmrE subunits may well be beyond the control of the membrane insertion machinery. EmrE dual topology is proposed to substantiate novel pathways for the evolution of membrane proteins. Therefore, resolution of the controversy has implications transcending the importance of multidrug transport.

We used spin labeling and electron paramagnetic resonance (EPR) spectroscopy (*14*) to derive structural constraints that describe the packing of the two EmrE monomers. In this report, we focus on representative sites near the 2-fold symmetry axis with proximity patterns that are inconsistent with antiparallel monomer packing. This is illustrated in helix 3, where the EPR spectrum at residue 60 near the N-terminal end of the helix shows distinct features arising from dipolar coupling between spin labels separated by less than 15 Å (Figure 1A). On the C-terminal side of the helix, EPR spectra of spin labels introduced at position 75 show broadening also characteristic of proximity in the 10−15 Å range. Double electron electron resonance (DEER) (*15*) analysis (Figure S1) reveals a bimodal distance distribution with a component separated by 15 Å (Figure 1B). An antiparallel arrangement of helix 3 predicts that the symmetry-related residues at its N- and C-termini are on opposite sides of the bilayer separated by 30−40 Å (Figure 1C). Similarly, the pattern of proximity at successive helical turns of helix 2 (residues 40, 44, and 47) is consistent with a parallel arrangement.

The presence of two spin label populations each separated by a different distance in the representative EPR spectra of Figure 1 was previously interpreted at site 14 as evidence

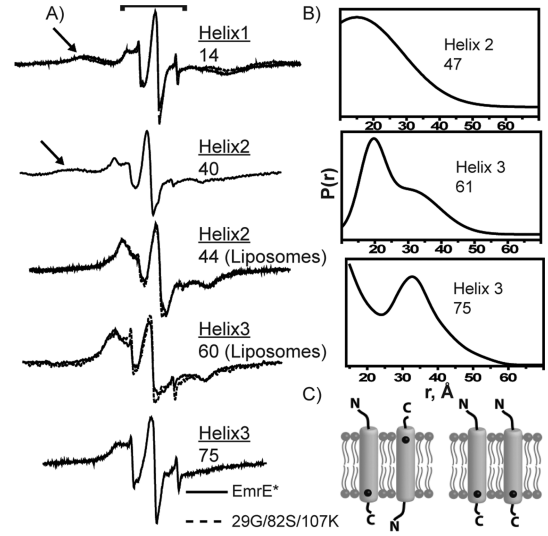

FIGURE 1: (A) Representative EPR spectra of spin labels at residues near the 2-fold symmetry axis. At sites 14 and 40, there is a distinct spectral feature (indicated by the arrow) that arises from very close (<8 Å) dipolar coupling. At sites 44, 60, and 75, dipolar coupling in the 15 Å range is manifested by an overall broadening of the lineshape. The bracket highlights the component of the EPR spectrum arising from spin labels separated by more than 20 Å. Scan widths are 250G for 14, 200G for 40, 44 and 60 and 160G for 75. (B) Representative distance distributions between symmetry-related spin labels in the dimer. (C) Pattern of proximity between N- and C-terminal residues of a pair of helices packed in parallel or antiparallel fashion.

* To whom correspondence should be addressed: Vanderbilt University, 741 Light Hall, Nashville, TN 37232-0615. Phone: (615) 322-3307. Fax: (615) 322-7236. E-mail: hassane.mchaourab@vanderbilt.edu.

10.1021/bi800628d CCC: $40.75
Published on Web 07/11/2008

of conformational heterogeneity (*6*). The expanded data set reveals multiple populations in other regions of EmrE, particularly helix 3. Because DEER is selective for doubly labeled dimers, The substantial difference in the distance for each spin population may reflect two or more EmrE conformers in equilibrium.

More importantly, we found that the packing interface is not sensitive to mutations that change the asymmetric charge distribution, the (K+R) bias, to favor a unique C_{in} orientation (Figure S2). The S107K, R29G/R82S, and R29G/R82S/S107K mutations do not alter the proximity between the spin labels as deduced from the superimposable EPR spectra (shown in Figure 1 for the triple mutant). To the extent that the proximities fingerprint the packing of their respective helices in the dimer, they indicate that the interface between the monomers remains intact regardless of the mutations. Furthermore, analysis by size-exclusion chromatography (SEC) reveals that the putative C_{in} mutants are homogeneous and have retention times very similar to that of WT-EmrE*. Overall, the EPR constraints disagree with the fundamental corollary of the dual topology model. If the dimer interface involves two antiparallel monomers, then forcing a unique membrane topology, through manipulation of the (K+R) bias, would hinder assembly of the dimer. Unless the monomer of EmrE is an independent folding unit, it will misfold and likely aggregate. The EPR spectra would be exquisitely sensitive to the disruption of the interface or to nonspecific interactions.

Previous work explored the effects of (K+R) bias on the location of GFP and PhoA C-terminal tags and the drug resistance phenotype conferred by EmrE mutants (*9*). The conclusion that EmrE assembles into an antiprallel dimer was based on two fundamental assumptions. First, GFP fluorescence is only determined by its location in either the cytoplasm or the periplasm (*16*). Thus, variations in whole cell GFP fluorescence intensity induced by manipulation of the EmrE (K+R) bias reflect a change in the location of the C-terminus. However, GFP fluorescence is also dependent on the efficient folding of the tagged protein (*17*). Thus, differences in levels of fluorescence between mutants may also reflect misfolding of the chimeras. Second, the membrane insertion efficiency of all the mutants is similar (*9*), although a direct analysis of membrane insertion was not performed. If this assumption is not tenable, then the reported functional complementation between oppositely oriented EmrE cannot be unequivocally interpreted as being indicative of an antiparallel dimer.

To test the correlation between (K+R) bias and GFP fluorescence, we characterized an expanded set of topology mutants (Figure S2). The substitutions were introduced into a background that consists of His-EmrE* (C39A/C41A/C95A) linked to cerulean fluorescent protein (CFP) (*18*) by the sequence GGSGG. The highly fluorescent chimeras reported by Rapp et al. are primarily based on the R29G substitution which by itself induces more than 90% of the observed increase in GFP fluorescence (*9, 19*), while the C_{out} mutants are based on L85R. We found that the nature of the substitution profoundly alters the level of insertion of the protein into the membrane (Figure 2A) and that the mutants partition into inclusion bodies (Figure S3), cytoplasmic fractions (data not shown), and membrane fractions (Figure 2A). The R29G-based mutants have a substantially higher level of protein in the membrane than the L85R mutant.

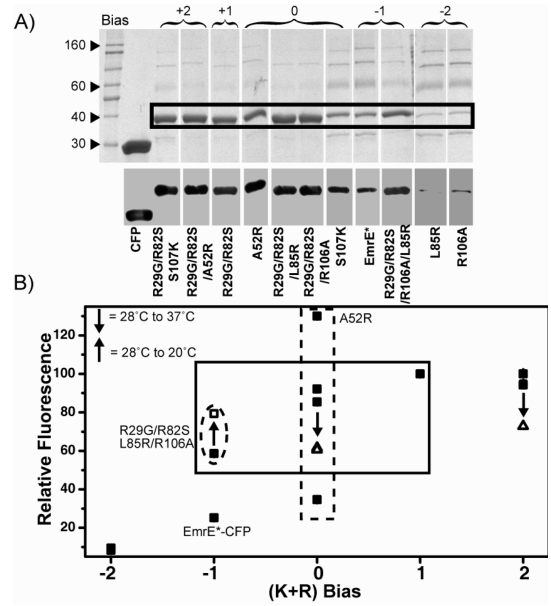

FIGURE 2: (A) SDS−PAGE analysis of nominally equal amounts of purified, membrane-inserted EmrE-CFP showing the variability in yield. Western blot analysis (bottom panel) with antibodies against the C-terminal CFP or N-terminal His tag (Figure S4) demonstrates the lack of proteolytic cleavage of the membrane-inserted chimeras. (B) (K+R) bias is not a unique determinant of EmrE*-CFP fluorescence. The data points represent the average of three measurements of CFP fluorescence emission at 520 nm (excitation at 440 nm). The error bars are within the width of each symbol. The solid box highlights fluorescence values of mutants bearing the R29G mutation. Three of the mutants were expressed either at 37 (△) and 28 °C (■) or at 28 (■) and 20 °C (□). The direction of change in fluorescence is indicated by the arrows. The (K+R) bias of EmrE*-CFP is −1 (Figure S1).

For the K and R mutants previously reported, the emission intensity of CFP is in qualitative agreement with the ranking from whole cell fluorescence (*11*). However, little change in relative quantum yield is observed when either L85R (−1) or R106A (−1) is introduced onto the R29G/R82S (+2) background for the purpose of reversing the change in bias and thus reducing the fluorescence intensity of CFP. Purified R29G/R82S-based EmrE*-CFP mutants, including R29G/R82S/L85R/R106A which has a bias identical to that of EmrE*-CFP, are fluorescent regardless of the overall bias (Figure 2B, solid box). Furthermore, four 0-bias chimeras constructed using independent mutations have substantially different levels of CFP fluorescence (Figure 2B, dashed box). The level of fluorescence is inversely related to the expression temperature, suggesting that thermodynamic stability is a contributing factor (Figure 2B, empty symbols). Overall, the data demonstrate that the (K+R) bias is not a unique determinant of CFP fluorescence. Analysis by SEC reveals that weakly fluorescent chimeras are not homogeneous, consisting of at least two protein populations, one of which is nonfluorescent. The CFP moieties in the dark chimeras have absorption spectra similar to those of acid-denatured CFP (Figure S5).

The dual topology model predicts that EmrE mutants biased toward a unique orientation will not assemble into functional dimers that translocate substrates out of the cytoplasm. Experimentally, resistance phenotypes conferred

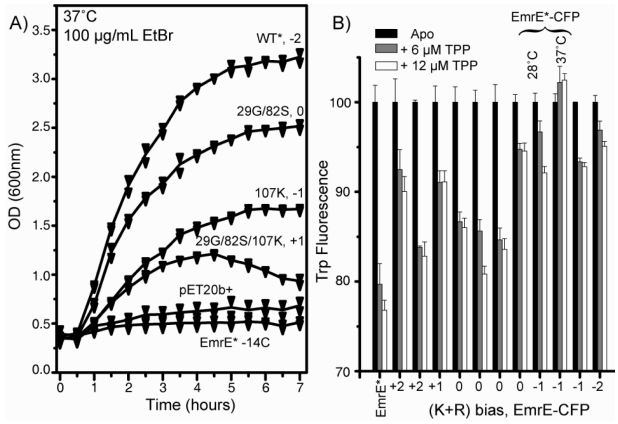

FIGURE 3: (A) Growth of *E. coli* transformed with the untagged EmrE* constructs in the presence of 0.25 mM (100 μg/mL) EtBr. The average and the individual points are displayed. (B) EmrE*-CFP mutants bind TPP as deduced from the quenching of Trp fluorescence (*23*). For EmrE*-CFP, increasing the expression temperature to 37 °C eliminates binding (shown by the bracket).

by untagged (neither His nor CFP) EmrE* mutants (Figure 3A) do not follow the (K+R) sequence bias. In particular, the putative N_{in}-C_{in} mutant, R29G/R82S/S107K, confers measurable resistance to EtBr when expressed under the control of a leaky promoter. This is evident by comparison to *E. coli* cells harboring the deactivated E14C mutant both at 30 °C (data not shown) and at 37 °C (Figure 3A). The asymptotic decrease in cell density likely reflects the toxicity of the triple mutant also detected by a slower growth rate in the absence of EtBr (data not shown). The resistance phenotype conferred by the triple mutant, even at a lower level compared to EmrE*, indicates intact assembly of the dimer despite the change in (K+R) bias. It is also consistent with in vitro TPP binding of purified C_{in}-biased constructs of EmrE*-CFP (Figure 3B) and EmrE*-S107K, EmrE*-R29G/R82S, and EmrE*-R29G/R82S/S107K (Figure S6).

The differences between our results and those of Rapp et al. (*9*) highlight the confounding factors that influence cell density, including the toxicity of the protein, the level of expression, the affinity of EmrE for EtBr, and rate of transport relative to the inward leak of EtBr. Given the observation that the putative C_{in} substitutions do not abolish the activity of EmrE, the functional complementation between C_{in} and C_{out} mutants cannot be unequivocally interpreted as evidence of dual topology. Despite compelling bioinformatics evidence of an antiparallel topology in SMR heterodimers (*9, 19*), the extension of this model to EmrE is not supported by experimental evidence. Most EmrE mutants (*9, 19*) with mixed N- and C-terminal orientations have inconsistent levels of GFP and PhoA activities (*20*). The simplest interpretation of these results is that each of the two tags, GFP and PhoA, affects the folding and possibly topological location of the N- and C-termini of EmrE in independent ways. Our set of topology mutants challenges the conclusion that the (K+R) bias of EmrE is necessary and sufficient for CFP fluorescence changes.

On the basis of the results presented in this paper, we propose that the favorable energetics of helix−helix interactions in the parallel dimer override an unfavorable (K+R) bias in the near-neutral region leading to a native N_{in}-C_{in} orientation. The analysis of Rapp et al. (*9*) considers asymmetric charge distribution as the only determinant of monomer topology in the dimer. In support of our model, it has been noted that for some transmembrane helices folding and insertion are context-dependent (*21, 22*). Interaction with neighboring helices, sequence context, and lipid interaction are among the determinants of membrane partitioning.

ACKNOWLEDGMENT

We acknowledge Drs. David Piston and GertJan Kremers for discussions of CFP fluorescence, Dr. Ben Spiller for discussions on membrane protein folding, Dr. Al Beth for critical reading of the manuscript, and Jared Godar for help with the figures.

SUPPORTING INFORMATION AVAILABLE

Experimental methods for sample preparation and analysis (Figures S1−S6). This material is available free of charge via the Internet at http://pubs.acs.org.

REFERENCES

1. Schuldiner, S., Granot, D., Mordoch, S. S., Ninio, S., Rotem, D., Soskin, M., Tate, C. G., and Yerushalmi, H. (2001) *News Physiol. Sci. 16*, 130–134.
2. Schuldiner, S. (2007) *Trends Biochem. Sci. 32*, 252–258.
3. Butler, P. J. G., Ubarretxena-Belandia, I., Warne, T., and Tate, C. G. (2004) *J. Mol. Biol. 340*, 797–808.
4. Fleishman, S. J., Harrington, S. E., Enosh, A., Halperin, D., Tate, C. G., and Ben-Tal, N. (2006) *J. Mol. Biol. 364*, 54–67.
5. Chen, Y.-J., Pornillos, O., Lieu, S., Ma, C., Chen, A. P., and Chang, G. (2007) *Proc. Natl. Acad. Sci. U.S.A. 104*, 18999–19004.
6. Koteiche, H. A., Reeves, M. D., and McHaourab, H. S. (2003) *Biochemistry 42*, 6099–6105.
7. Ubarretxena-Belandia, I., Baldwin, J. M., Schuldiner, S., and Tate, C. G. (2003) *EMBO J. 22*, 6175–6181.
8. Ma, C., and Chang, G. (2007) *Proc. Natl. Acad. Sci. U.S.A. 104*, 3668.
9. Rapp, M., Seppala, S., Granseth, E., and von Heijne, G. (2007) *Science 315*, 1282–1284.
10. Ninio, S., Elbaz, Y., and Schuldiner, S. (2004) *FEBS Lett. 562*, 193–196.
11. Schuldiner, S. (2007) Controversy over EmrE structure. *Science 317*, 748–751.
12. Steiner-Mordoch, S., Soskine, M., Solomon, D., Rotem, D., Gold, A., Yechieli, M., Adam, Y., and Schuldiner, S. (2008) *EMBO J. 27*, 17–26.
13. von Heijne, G. (1986) *EMBO J. 5*, 3021–3027.
14. Hubbell, W. L., Mchaourab, H. S., Altenbach, C., and Lietzow, M. A. (1996) *Structure 4*, 779–783.
15. Pannier, M., Veit, S., Godt, A., Jeschke, G., and Spiess, H. W. (2000) *J. Magn. Reson. 142*, 331–340.
16. Feilmeier, B. J., Iseminger, G., Schroeder, D., Webber, H., and Phillips, G. J. (2000) *J. Bacteriol. 182*, 4068–4076.
17. Pedelacq, J.-D., Cabantous, S., Tran, T., Terwilliger, T. C., and Waldo, G. S. (2006) *Nat. Biotechnol. 24*, 79–88.
18. Malo, G. D., Pouwels, L. J., Wang, M., Weichsel, A., Montfort, W. R., Rizzo, M. A., Piston, D. W., and Wachter, R. M. (2007) *Biochemistry 46*, 9865–9873.
19. Rapp, M., Granseth, E., Seppala, S., and von Heijne, G. (2006) *Nat. Struct. Mol. Biol. 13*, 112–116.
20. Daley, D. O., Rapp, M., Granseth, E., Melen, K., Drew, D., and von Heijne, G. (2005) *Science 308*, 1321–1323.
21. Hessa, T., Meindl-Beinker, N. M., Bernsel, A., Kim, H., Sato, Y., Lerch-Bader, M., Nilsson, I., White, S. H., and von Heijne, G. (2007) *Nature 450*, 1026–1030.
22. von Heijne, G. (2007) *J. Gen. Physiol. 129*, 353–356.
23. Elbaz, Y., Tayer, N., Steinfels, E., Steiner-Mordoch, S., and Schuldiner, S. (2005) *Biochemistry 44*, 7369–7377.

BI800628D